Development of a Nonlinear Statistical Method for Estimating the Downward Longwave Radiation at the Surface from Satellite Observations

HAI-TIEN LEE AND ROBERT G. ELLINGSON*

Cooperative Institute for Climate Studies, Department of Meteorology, University of Maryland, College Park, Maryland

(Manuscript received 2 November 2001, in final form 5 March 2002)

ABSTRACT

This paper develops a nonlinear statistical method that uses satellite radiance observations directly to estimate the downward longwave radiation (DLR) at the earth's surface, a necessary component of the surface energy budget. The proposed technique has rms regression errors of about 9 W m^{-2} for clear-sky conditions, and about 4 to 8 W m^{-2} for overcast conditions, depending on the cloud levels. It is shown that this technique can produce unbiased estimates over a large range of meteorological conditions, which is crucial for climate studies.

Sensitivity studies show that the DLR is most sensitive to errors in the cloud amount on average. Overall, the combined errors for an instantaneous DLR estimate, excluding the effects of the surface pressure errors, range from about 7 to 12 W m^{-2} when there is a $\pm 10\%$ uncertainty in cloud amount and a ± 100 hPa uncertainty in cloud-base pressure. When the cloud amount uncertainty rises to 30%, the combined DLR error ranges from about 10 to 25 W m^{-2}.

This clear-sky DLR estimation technique was validated preliminarily by using simulated radiation data. The DLR differences between estimated and calculated values have a standard deviation of about 9 W m^{-2} and are unbiased in most conditions.

The validity of the DLR estimation technique has been demonstrated; however, validation for cloudy conditions, comparison with surface observations, and improvements related to surface pressure dependence and skin temperature discontinuity are left for future study.

1. Introduction

The surface energy budget plays an important role in determining many atmospheric and oceanic processes, especially on the large scale. The energy balance directly affects the boundary layers of both the atmosphere and the ocean. It influences their patterns of circulation and ultimately impacts the earth's climate system. The Global Energy and Water Cycle Experiment (GEWEX), among many scientific programs, has shown the need for a better estimation of the surface energy budget and called for an accuracy of 10 W m^{-2} in the net monthly average surface energy budget (WCRP-5 1988).

Recognizing this, several surface observation networks for continuously measuring in situ, long-term surface radiation have been established. The World Climate Research Program (WCRP) sponsors the Baseline Surface Radiation Network (BSRN) (Ohmura et al. 1998). The U.S. National Oceanic and Atmospheric Administration (NOAA) continues the radiation budget efforts through the Integrated Surface Irradiance Study (ISIS) (Hicks et al. 1996) and the Surface Radiation Budget Network (SURFRAD) (Augustine et al. 2000). The Atmospheric Radiation Measurement Program (ARM) (Stokes and Schwartz 1994), supported by the U.S. Department of Energy, is one of the most complete and sophisticated field experiments for this subject.

Various satellite-based methods for estimating the surface radiation have been developed starting mostly in the 1980s. Schmetz (1989) and Ellingson (1995) provide comprehensive reviews of those methods. As a partial list, algorithms that estimate the surface solar radiation include Tarpley (1979), Gautier et al. (1980), Pinker and Corio (1984), and Dedieu et al. (1987). For the surface thermal radiation, algorithms were developed by Smith and Woolf (1983), Darnell et al. (1983, 1986), Meerkoetter and Grassl (1984), Schmetz et al. (1986), Morcrette and Deschamps (1986), Frouin and Gautier (1988), Gupta et al. (1989, 1992, 1993, 1999) and Lee (1993).

The downward thermal radiation at the surface, herein referred to as the downward longwave radiation (DLR), is one of the components of the surface energy budget. Before the advent of satellite techniques, oceanographers and meteorologists studying air–sea interaction used the empirically derived ''bulk formulae'' with syn-

* Current affiliation: Department of Meteorology, The Florida State University, Tallahassee, Florida.

Corresponding author address: Dr. Hai-Tien Lee, Department of Meteorology, University of Maryland, College Park, MD 20742.
E-mail: lee@wam.umd.edu

optically observed parameters to estimate net terrestrial radiation (Fung et al. 1984). Some satellite techniques follow a similar path. The radiation quantities are determined by empirical functions using satellite-derived meteorological parameters, for example, the near-surface temperatures and water vapor burden. Their advantages are computational efficiency and ease of adaptation.

Another approach is to calculate the radiation quantities with radiative transfer models using satellite-derived soundings. A strong feature of this approach is the validity of the physics. However, it is the most costly due to the computationally intensive radiative transfer calculations. Therefore, models with different degrees of detail were developed to compromise this disadvantage. Note that the satellite meteorological data used by the above algorithms are all in the form of the retrieval products so that the error of the algorithms is subject to the retrieval accuracy.

This paper describes a new method that uses satellite-observed radiances directly to avoid the propagation of retrieval errors of meteorological parameters into the final radiation estimate. We embedded the physical merits of the radiative transfer within the parameterization of nonlinear functions of observed radiance. The forms of the nonlinear functions were determined using our best understanding of the physics involved, and necessary coefficients were statistically determined using least squares regression.

The DLR estimation algorithm developed in this study is for use with data from the second generation, high-resolution infrared spectrometer (HIRS/2) on board the NOAA *TIROS-N* series satellites (NOAA 1995). The intent is to develop the DLR estimation algorithm as a companion to the outgoing longwave radiation (OLR) technique (Ellingson et al. 1989) already developed for use with the HIRS series instruments on the NOAA operational polar orbiters. Although the current development is specifically for the *NOAA–10* HIRS/2, the extension to HIRS series instruments on the newer satellites is relatively easy, mainly involving optimal selection of spectral intervals and generation of the regression coefficients.

In the material that follows, section 2 describes the basic equations and radiation model calculations, section 3 describes the algorithm development, section 4 describes the sensitivity and error analysis, section 5 describes the preliminary validation results, and section 6 provides concluding remarks.

2. Basic equations and radiation model calculations

a. Basic equations

The upwelling radiance N observed from a satellite is related to the specific intensity I_ν at a given local zenith angle θ as

$$N_i(\mu) = \int_{\Delta\nu_i} I_\nu(z_t, \mu)\phi_i(\nu)\, d\nu, \tag{1}$$

where $\mu \equiv \cos\theta$, ϕ_i is the normalized response function for channel i, ν is the wavenumber or frequency, and z_t is the satellite altitude or the top of the atmosphere (assuming axial symmetry).

The upwelling clear column radiance for a plane parallel, horizontally homogeneous nonscattering atmosphere in local thermodynamic equilibrium above a black surface is related to the temperature and absorbing constituents as

$$I_\nu(z_t; \mu) = B^*_\nu(0)T_\nu(z_t, 0; \mu) + \int_0^{z_t} B_\nu(z')\frac{\partial T_\nu(z_t, z'; \mu)}{\partial z'}\, dz', \tag{2}$$

where $B^*_\nu(0)$ is the Planck function evaluated with the surface temperature, $B_\nu(z')$ is the Planck function evaluated with the temperature at level z', and the monochromatic transmittance $T_\nu(z_t, z'; \mu) \equiv e^{-(\tau_\nu(z') - \tau_\nu(z))/\mu}$, where τ_ν is the optical depth for the atmospheric absorbers [see Ellingson and Gille (1978), Ellingson and Ferraro (1983)].

Since liquid water clouds are almost opaque in the thermal infrared, the transmissivity through the cloud is nearly zero if the cloud thickness exceeds about 300 m. Therefore, the upwelling specific intensity for overcast conditions may be approximated as

$$I_{\nu,c}(z_t; \mu) = B_\nu(z_{ct})T_\nu(z_t, z_{ct}; \mu) + \int_{z_{ct}}^{z_t} B_\nu(z')\frac{\partial T_\nu(z_t, z'; \mu)}{\partial z'}\, dz', \tag{3}$$

where z_{ct} is the cloud-top height and the monochromatic transmittance is defined as above.

The DLR is related to the downward specific intensity $I_\nu(z = 0, -\mu)$ at the earth's surface in an axial-symmetric atmosphere as

$$\mathrm{DLR} = 2\pi \int_0^\infty \int_0^1 I_\nu(z = 0, -\mu)\mu\, d\mu\, d\nu. \tag{4}$$

For clear-sky conditions we can write

$$I_{\nu,0}(z = 0; -\mu) = -\int_0^{z_t} B_\nu(z')\frac{\partial T_\nu(0, z'; -\mu)}{\partial z'}\, dz'. \tag{5}$$

For overcast, infinitesimally thin, black, single-layer cloud conditions we can write

$$I_{\nu,c}(z = 0; -\mu) = B_\nu(z_{cb})T_\nu(0, z_{cb}; -\mu) - \int_0^{z_{cb}} B_\nu(z')\frac{\partial T_\nu(0, z'; -\mu)}{\partial z'}\, dz', \tag{6}$$

where z_{cb} is the cloud-base height.

For partial cloud conditions, assuming an infinitesi-

mally thin, single-layer cloud with amount A, the total DLR is commonly written as the cloud-amount-weighted sum of the DLR from clear and cloudy portions of the sky, respectively, as

$$\mathrm{DLR} = (1 - A)F_o^{\downarrow} + AF_c^{\downarrow}, \quad (7)$$

where $F_o^{\downarrow}$ and $F_c^{\downarrow}$ are the downward longwave fluxes at the surface from the clear and cloudy portions of sky, respectively. For nonblack clouds, A is the effective fractional cloud amount, which is defined as the product of the cloud emissivity and the absolute fractional cloud amount. The geometric effects of the cloud can be generalized into this form (Ellingson 1982) and this expression can be generalized for a multilayer stratified cloud system as well.

b. Radiative transfer calculations

We use a radiative transfer model to simulate the DLR and upwelling clear-sky radiances, as needed to determine the statistical models. These models were first reported by Ellingson and Gille (1978) and updated by Ellingson and Serafino (1984) and Ellingson et al. (1994; hereafter referred as RGE model). This model has been tested in the Intercomparison of Radiation Codes for Climate Models (ICRCCM, see Ellingson et al. 1991), and also with observations. Although the absolute accuracy has not been established, the model has been shown to produce the OLR and DLR calculations that agree with line-by-line calculations to within about $\pm 2\%$. OLR from regression instantaneous estimates based on this model's HIRS data have shown agreement with Earth Radiation Budget Experiment (ERBE) to within 4 W m^{-2} (Ellingson et al. 1994). Furthermore, Ellingson and Serafino (1984) showed agreement with aircraft-OLR and surface-DLR data to within the accuracy of the observations.

This radiative transfer model has 140 spectral intervals across 0–3000 cm^{-1} with interval widths varying from 5 cm^{-1} to 40 cm^{-1} depending on their locations in the spectrum. It includes five gases: water vapor (H_2O), ozone (O_3), carbon dioxide (CO_2), nitrous oxide (N_2O), and methane (CH_4). For the purpose of this study, the carbon dioxide concentration is assumed constant at 330 ppm by volume. It should be pointed out that the model tests indicate a 0.2 W m^{-2} underestimate using this as compared with 360 ppm. Concentrations of N_2O and CH_4 are also assumed constant at 0.279 and 1.75 ppm, respectively.

The Malkmus random band model (Malkmus 1967) was used for the local lines of all of the gases. The water vapor continuum is included using the parameterization followed by Clough et al. (1989). The effect of overlapping absorptions from different gases is calculated as the product of the individual transmissivities.

We used the NOAA-supplied, laboratory-measured values of HIRS/2 response functions to simulate the nadir upwelling clear-column radiances at the top of the atmosphere for all HIRS/2 channels by trapezoidal integration of Eq. (1). We calculated the DLR at the surface with the angular and frequency integrations of the corresponding intensities (see Eq. 4). A four-point Gaussian quadrature was used to perform the integration over the angles. The DLR for overcast conditions was simulated by setting the cloud base at different pressure levels, with a cloud emissivity of one, and keeping the temperature and water vapor profiles unchanged [see Eq. (6)].

Following our research on the OLR (Ellingson et al. 1989), we used a set of 1600 soundings compiled by Phillips et al. (1988) as input to the radiative transfer model. Each sounding includes temperature values at 65 different pressure levels from 0.1 to 1000 hPa and the mixing ratios of H_2O and O_3 in the corresponding 64 layers. The soundings were compiled from radiosondes ascents from land and ocean stations between 30°S and 60°N in latitude, and the soundings are equally divided between tropical (30°S–30°N) and midlatitude, winter and summer conditions. The O_3 data were chosen by Phillips et al. to be climatologically consistent with the temperature profiles, and the stratospheric H_2O mixing ratio is assumed to be 3 ppm. The earth's skin temperature and the surface air temperature are assumed equal.

3. Algorithm development

Theoretically one can calculate the DLR using a radiative transfer model, given temperature and atmospheric gas profiles. From satellite observations, existing temperature and water vapor retrieval techniques can provide the needed information for such models to proceed to global DLR studies. Highly parameterized radiative transfer physical models designed to use satellite-inferred information have been well developed (Darnell et al. 1983; Gupta 1989; Frouin and Gautier 1988; Schmetz et al. 1986). Rather than using satellite retrieval data in physical models, some developers use satellite data in statistical models. For example, Gupta (1989) developed a statistical algorithm based on radiation model calculations for use with TIROS Operational Vertical Sounder (TOVS) sounding retrievals, and adapted it for specific use with the International Satellite Cloud Climatology Project C1 ISCCP C1dataset (Gupta et al. 1992), where the satellite-inferred temperature, water vapor, and better cloud data are provided. Their recent work can be found in Gupta et al. (1993, 1999).

Our approach to the DLR estimation is also statistical. However, we explored the possibility of using satellite observations directly instead of their inferred quantities, such that it is possible to reduce the error of DLR estimation that propagates from the retrievals. Furthermore, the computational speed of statistical models is superior compared to physical models. This feature is important for operational implementation and for using

historical data to derive the radiation budget climatology.

There is a problem when using satellite-observed radiance if clouds are present in the field of view of the satellite-borne radiometer. The clouds contaminate the information about the temperature and absorbing gas concentration distributions. In addition, when clouds are optically thick there is little information concerning cloud base and the atmospheric conditions below the clouds. The DLR contributed by the clouds cannot be estimated very well by the cloud-contaminated upwelling radiance unless information below the cloud is provided by other means.

The cloud-clear radiance, or the clear-column radiance, is mostly inferable, and is operationally derived from radiance observations (Smith and Woolf 1976; McMillin 1978; McMillin and Dean 1982). The clear-column radiance, when obtainable, contains information about the entire atmospheric column, particularly information about the near-surface temperature and water vapor fields that are the most important parameters for estimating the DLR. However, the cloud-clearing process can only be carried out in partly cloudy scenes due to the requirement that the algorithm find adjacent pair of HIRS pixels that are identified as having clouds at the same height but with different cloud amounts. That means whenever an area is under an overcast, the clear-column radiance will not be available. As an example, a HIRS clear-column radiance dataset for the period from 14 December 1990 to 14 January 1991 gives about 82% of daily global coverage with both orbits. The global spatial coverage rises to 91% when 14 days of data are superimposed on a 2.5° × 2.5° grid, and it reaches 97% for 32 days. Except for geographical regions where it is persistently overcast, it is legitimate to say that the global coverage of clear-column radiance is sufficient for the study of monthly mean DLR.

Although the technique that uses a linear combination of the satellite-observed radiances to estimate the OLR has been proven successful (Ellingson et al. 1989, 1994), the DLR estimation using these radiances is not physically as straightforward as the OLR estimation. Even though it is possible to estimate the DLR from a linear combination of clear-column radiances, as will be shown in section 3a, it is completely unconnected physically.

Mathematically, one cannot find an analytical expression for the DLR in terms of the clear-column radiances except for assumed dependence of the atmospheric structure (e.g., isothermal condition or the thermal emission is linear in the optical depth) because they are all complicated functionals [see Eqs. (2)–(6)]. However, physically we do know that the clear-column radiances contain information related to the DLR (i.e., the information of the vertical structures of temperature and water vapor). In section 3b we develop a nonlinear statistical model that is physically connected to the radiative transfer.

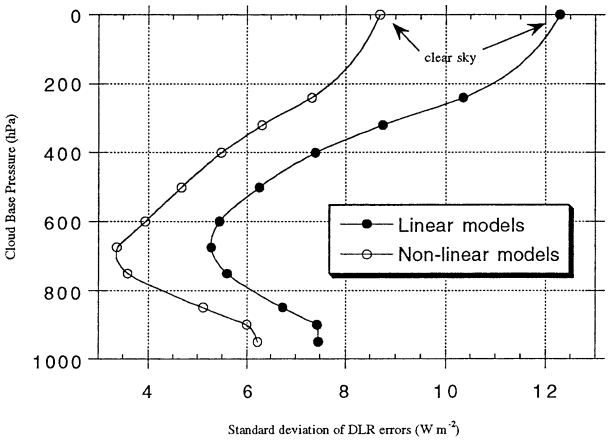

FIG. 1. DLR regression error for clear and overcast sky conditions by linear and nonlinear models plotted with the corresponding cloud-base pressure.

a. Linear model

As the simplest, yet physically unconnected, estimation model of the DLR, we expressed the DLR as a linear sum of HIRS radiances, namely,

$$F_o^{\downarrow} = a_o + \sum a_i N_i \tag{8}$$

$$F_c^{\downarrow}(p_{\rm cb}) = b_o(p_{\rm cb}) + \sum b_i(p_{\rm cb}) N_i, \tag{9}$$

where $F_o^{\downarrow}$ and $F_c^{\downarrow}$ are the DLR at the surface from the clear and cloudy portions of sky, respectively; N_i is the clear-column radiance of HIRS channel i, $p_{\rm cb}$ is the cloud-base pressure, a_0, and a_i, b_0, and b_i are regression coefficients.

The stepwise regression procedure (IMSL 1989) chose HIRS channels 5, 6, 7, 8, 10, and 11 for both Eqs. (8) and (9). The rms regression errors of this model range from about 5 to 12 W m^{-2} as shown by Fig. 1. With these six channels, the model explains more than 97% of variances. Note that the clear-sky case has the largest rms regression error. This is related to the magnitudes of the explained variances and the DLR variances of different sky conditions.

It is somewhat complicated to explain why the clear-sky DLR has a higher variance than the overcast DLR. Some insight is obtained by examining a simple approximation to the DLR. For an isothermal atmosphere, the clear-sky DLR, $F_{\rm clr}$, can be expressed as $F_{\rm clr} = (1 - T_{\rm atm})F_{\rm cld}$, where $F_{\rm cld}$ is the DLR for the overcast sky and $T_{\rm atm}$ is the atmospheric column flux transmissivity.

Outside the window regions where the atmosphere is near opaque, the clear-sky DLR is approximately equal to the overcast DLR; and therefore the clear-sky and overcast DLR have about equal variances. However, for the window regions, if we approximate the atmospheric emissivity as a linear function of the total precipitable water, it is possible to derive an analytic expression for the variances of clear-sky and overcast DLR. It can be seen that the difference between the clear-sky and over-

cast DLR variances is a function of the variance of precipitable water, the variance of the cloud-base temperature, and the covariance of the precipitable water and cloud-base temperature. It is the state of the atmosphere that determines if the clear-sky DLR has a larger variance than the overcast one. For example, if the air temperatures were fixed, the variance of the clear-sky DLR will be larger than overcast DLR, because the overcast DLR in an isothermal atmosphere depends only on temperature; conversely, if the precipitable water were fixed, the overcast DLR variance will be the larger of the two.

From our DLR calculations, the clear-sky DLR has a larger variance. In overcast conditions, the mean temperature between the cloud base and the surface dominates the window region DLR reaching the surface; and this can be better estimated by the HIRS radiances than the variations in the temperature and water vapor in the clear-sky atmospheric column.

The HIRS channels chosen for the clear-sky regression model are qualitatively linked with the physics governing the DLR. Outside of the window regions, the absorption coefficients of the active absorbers are large and the densities of these absorbers are large enough to prohibit a contribution from the atmosphere beyond about 100 m above the surface. The window region is more sensitive to variations in temperature and water vapor away from the surface due to the small absorption and emission. Nonetheless, due to the near exponential decrease of the water vapor density with altitude, most of the DLR originates from the lowest few hundred meters of the atmosphere and is determined by the corresponding temperature and the water vapor content (Ellingson 1995). The stepwise regression did choose the channels that are strongly correlated with the near-surface temperature or the water vapor content. The first channel chosen was channel 8, which is centered at about 11.1 μm. It is very sensitive to the surface temperature since it is located in the 10-μm atmospheric window. The second channel chosen was channel 10, which is centered at about 8.2 μm. It is located in the wing of the 6.3-μm water vapor band and therefore is sensitive to the lower-tropospheric water vapor amount as well as the near-surface temperature. Although these two channels explain about 89% of the total variance, the addition of the next four channels still made significant improvement.

The channels containing the water vapor information are also strongly influenced by temperature variations. The variation of the radiance corresponding to the variation of the water vapor content is likely obscured by the variation of the temperature. Therefore the temperature variation may dominate the model statistically and the water vapor variation would not be correctly modeled. For this reason, we checked to see if this model is equally responsive to both temperature and water vapor variations.

Figures 2a–c show the residuals of calculated DLR minus that predicted from the linear regression model for clear skies (Eq. 8), as functions of the predicted DLR, surface temperature (T_s), and the total column precipitable water (PW), respectively. Although Fig. 2a shows little correlation between the residual and the predicted DLR, Fig. 2c shows the residuals increase as the water vapor burden increases. For very hot surfaces, Fig. 2b suggests the DLR will be consistently overestimated.

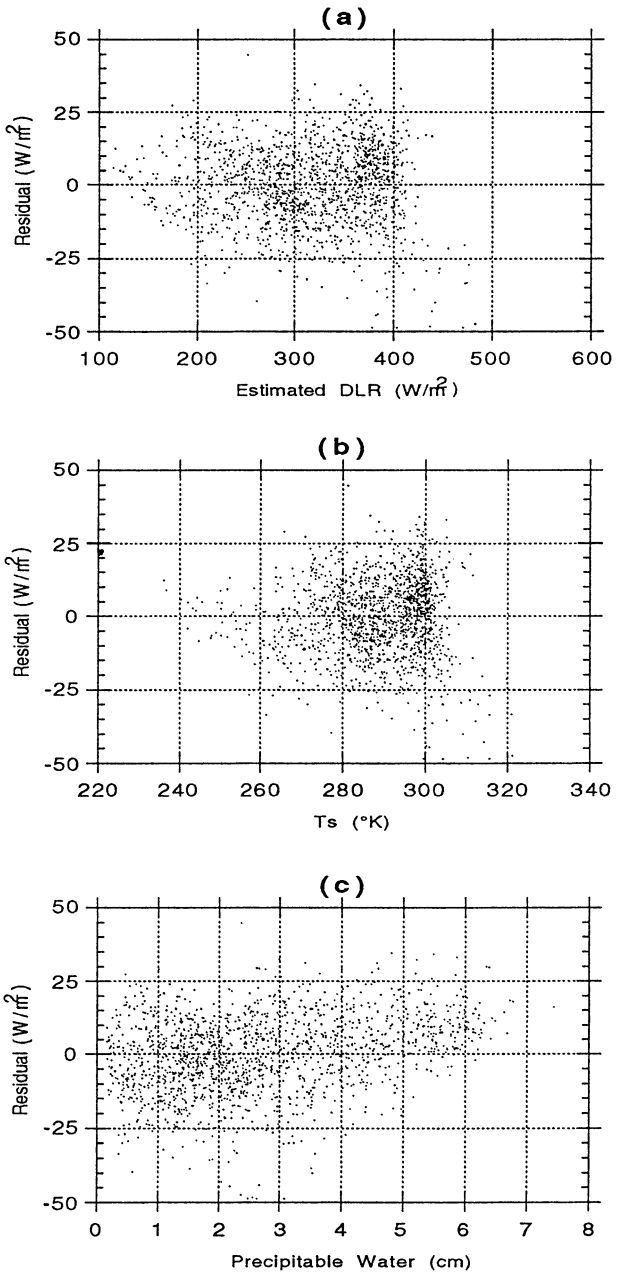

FIG. 2. Residuals of calculated DLR minus that predicted from the linear regression model for clear skies plotted against (a) predicted DLR, (b) surface temperature, and (c) total column precipitable water.

Several other linear model forms were attempted, in-

cluding cross-products of the radiances as the predictors. Nevertheless, all of them have similar problems to the linear model discussed earlier. These results prompted a nonlinear approach.

b. Nonlinear model

From Eq. (4), the monochromatic downward longwave flux from a clear sky can be expressed as

$$F^{\downarrow}_{\nu,o} = -\int_0^{z_t} \pi B_\nu(z') \frac{\partial T_{F\nu}(0, z')}{\partial z'}\, dz', \qquad (10)$$

where $T_{F\nu}(0, z') \equiv 2\int_0^1 T_\nu(0, z'; \mu)\mu\, d\mu$ is the monochromatic flux transmittance of the atmosphere. One can always find an effective temperature such that

$$F^{\downarrow}_{\nu,o} = \pi \overline{B}^{(0,z_t)}_{\nu} \varepsilon_{F\nu}(0, z_t), \qquad (11)$$

where $\varepsilon_{F\nu} = 1 - T_{F\nu}$ is the monochromatic flux emittance of the atmosphere, and the effective temperature is defined by

$$\pi \overline{B}^{(0,z_t)}_{\nu} \equiv \frac{-\int_0^{z_t} \pi B_\nu(z') \frac{\partial T_{F\nu}(0, z')}{\partial z'}\, dz'}{\varepsilon_{F\nu}(0, z_t)} \qquad (12)$$

A similar expression for an overcast sky with a single black cloud layer at an altitude z_c is

$$F^{\downarrow}_{\nu,z_c} = \pi B_\nu(z_c) T_{F\nu}(0, z_c) + \pi \overline{B}^{(0,z_c)}_{\nu} \varepsilon_{F\nu}(0, z_c) \quad \text{or} \quad (13)$$

$$F^{\downarrow}_{\nu,z_c} = \pi B_\nu(z_c) + \varepsilon_{F\nu}(0, z_c)(\pi \overline{B}^{(0,z_c)}_{\nu} - \pi B_\nu(z_c)). \quad (14)$$

Here, $\varepsilon_{F\nu}(0, z')$ can be considered as the emissivity of the atmosphere in the layer between surface and z'. $\overline{B}^{(0,z_c)}_{\nu}$ is defined similarly to (12) by replacing z_t with z_c. It represents an effective emitting temperature for the layer between the surface and the cloud base.

Note that for clear-sky conditions, Eq. (11) may be written as $\varepsilon\sigma T_e^4$ when integrated over the full spectrum, where ε is the emissivity of the atmosphere for the given temperature and moisture profiles, σ is the Stefan–Boltzmann constant, and T_e is an effective radiating temperature of the atmosphere. However, Eq. (11) cannot be applied directly to calculations since we do not have an a priori definition for the effective temperature unless the atmospheric emissivity is known. In order to define the effective temperature and also separate the water vapor dependence from temperature effects, we define the effective temperature with the brightness temperatures from HIRS channels and empirically specify the atmospheric emissivity as a function of the total precipitable water, wishing to have correct modeling of the dependence on water vapor.

To experiment with this idea, an atmospheric emissivity for a HIRS channel is defined based on the its brightness temperature by

$$\varepsilon_k = \frac{F^{\downarrow}_o}{\sigma T_k^4}, \qquad (15)$$

where the subscript k denotes the channel number and $F^{\downarrow}_o$ is the clear-sky DLR. The top of atmosphere brightness temperature T_k is determined from the inverse of the Planck radiation equation for a given channel radiance.

Since most of the DLR originates in the lowest few hundred meters of the atmosphere, we expect that the brightness temperatures of the channels that are sensitive to the near surface will best represent the effective temperature. Figure 3 shows the emissivities defined by Eq. (15) using brightness temperatures from channels 8, 10, and 13, respectively, plotted as functions of the precipitable water. One can expect that the functional form would be relatively simple with small fitting errors. Note that ε defined by Eq. (15) may have values larger than one because we use T_k as a surrogate for T_e.

We performed regression analysis with the clear-sky DLR expressed as

$$F^{\downarrow}_o = \sigma T_k^4 (a_0 + a_1 \mathrm{PW} + a_2 \sqrt{\mathrm{PW}}) \qquad (16)$$

considering that PW might be derivable from the radiances.

Using either channels 8, 10, or 13 for T_k, we obtained an rms error of about 5 W m^{-2}—a halving of the errors of the linear model! This is because the most variable parameter, the columnar water vapor, was prescribed accurately. Regardless, the DLR residuals are now distributed uniformly over the entire range of water vapor content, implying that this approach did achieve a more correct response to the water vapor variation. With the separation of the major temperature and water vapor dependencies, the earlier model expression is successful in interpreting the temperature and water vapor variations equally. This formulation is readily applicable once an accurate estimation of precipitable water is provided. However, for our purpose, we need to devise a method to estimate the emissivity from the HIRS data.

To formulate representations of water vapor by the radiances, we considered the ratios of radiances from two spectral intervals with different absorptivities in water vapor. During development, however, we found that the brightness temperature ratios give smaller regression errors and are more stable when instrument noise was introduced. We chose to use the channel 10 brightness temperature as the estimate of the effective temperature because it yielded the smallest regression errors, and it avoids sensitivity problems to the surface emissivity and potential skin–air temperature differences.

The nonlinear model for clear-sky conditions is written as

$$F^{\downarrow}_o = \sigma T_{10}^4 \left(a_0 + a_1 \sqrt{\frac{T_{13}}{T_{10}}} + a_2 \frac{T_{13}}{T_{10}} + a_3 \sqrt{\frac{T_{13}}{T_8}} + a_4 \sqrt{\frac{T_{13}}{T_7}} + a_5 \sqrt{T_8} + a_6 T_7 + a_7 T_8 \right), \qquad (17)$$

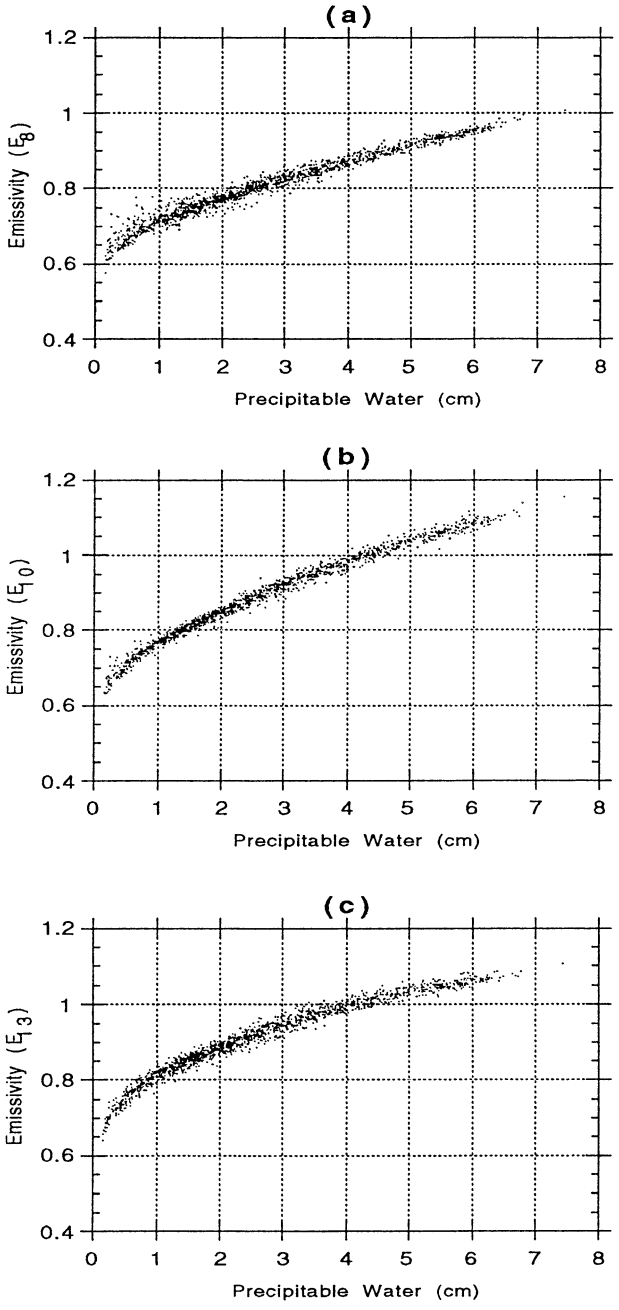

FIG. 3. Emissivity defined by Eq. (15) corresponding to HIRS channels (a) 8, (b) 10, and (c) 13, respectively, plotted as functions of the precipitable water.

where a_i are regression coefficients. Besides the first two temperature ratio terms in Eq. (17), which are related to the water vapor content [cf. Eq. (16)], the formulation was determined by stepwise regression analyses with candidate predictors expressed as different functions of the HIRS brightness temperatures.

The approach is a little different for overcast conditions. We take the difference between overcast and clear-sky DLR, that is, the cloud radiative forcing,

$$\Delta F^{\downarrow}_{\nu,z_c} = \pi B_\nu(z_c) T_{F\nu}(0, z_c) - \pi \overline{B}^{(z_c,z_t)}_{\nu} \varepsilon_{F\nu}(z_c, z_t), \quad (18)$$

where

$$\pi \overline{B}^{(z_c,z_t)}_{\nu} \equiv \frac{-\int_{z_c}^{z_t} \pi B_\nu(z') \dfrac{\partial T_{F\nu}(0, z')}{\partial z'} dz'}{\varepsilon_{F\nu}(z_c, z_t)}. \quad (19)$$

Since little DLR comes from the atmosphere above the cloud, the second term in Eq. (18) is negligible compared with the first term. We write Eq. (18) approximately as

$$\Delta F^{\downarrow}_{\nu,z_c} = \pi B_\nu(z_c) T_{F\nu}(0, z_c). \quad (20)$$

If the cloud-base temperature is known, the monochromatic flux transmittance may be defined as

$$T_{F\nu}(0, z_c) = \frac{\Delta F^{\downarrow}_{\nu,z_c}}{\pi B_\nu(z_c)}. \quad (21)$$

Without a priori knowledge of the cloud base, one must find a surrogate that best represents the cloud-base temperature. We empirically determined that the brightness temperature of channel 10 serves this purpose appropriately. Similar to Eq. (15) for spectrally integrated quantities, we define the atmospheric transmissivity by

$$T_F(0, z_c) = \frac{F^{\downarrow}_{c,z_c} - F^{\downarrow}_{o}}{\sigma T^4_{10}}, \quad (22)$$

where $F^{\downarrow}_{c,z_c}$ is the overcast sky DLR when a cloud base is at z_c.

Knowing that the brightness temperature from channel 10 does not necessarily represent the cloud-base temperature, the atmospheric transmissivity defined by Eq. (22) does show a nice functional dependence on the total precipitable water similar to that of the clear sky as shown in Fig. 3. Although the transmissivity in Eq. (22) is only for the layer between the surface and the cloud base, it still can be some function of the total precipitable water since most of the water vapor is located in the lowest part of the atmosphere.

Following the form developed for the clear-sky DLR, the regression analysis for the transmissivity was performed. Coincidentally, the exact same seven terms as in the clear-sky case were chosen, except that $\sqrt{T_{13}/T_7}$, $\sqrt{T_8}$, and T_7 are no longer significant when cloud-base pressure is lower than 600 hPa. The nonlinear model for estimating the DLR cloud radiative forcing is

$$\Delta F^{\downarrow}_{c,z_c} = \sigma T^4_{10}\Bigg(b_{0,z_c} + b_{1,z_c}\sqrt{\frac{T_{13}}{T_{10}}} + b_{2,z_c}\frac{T_{13}}{T_{10}} + b_{3,z_c}\sqrt{\frac{T_{13}}{T_8}} + b_{4,z_c}\sqrt{\frac{T_{13}}{T_7}} + b_{5,z_c}\sqrt{T_8} + b_{6,z_c}T_7 + b_{7,z_c}T_8\Bigg), \quad (23)$$

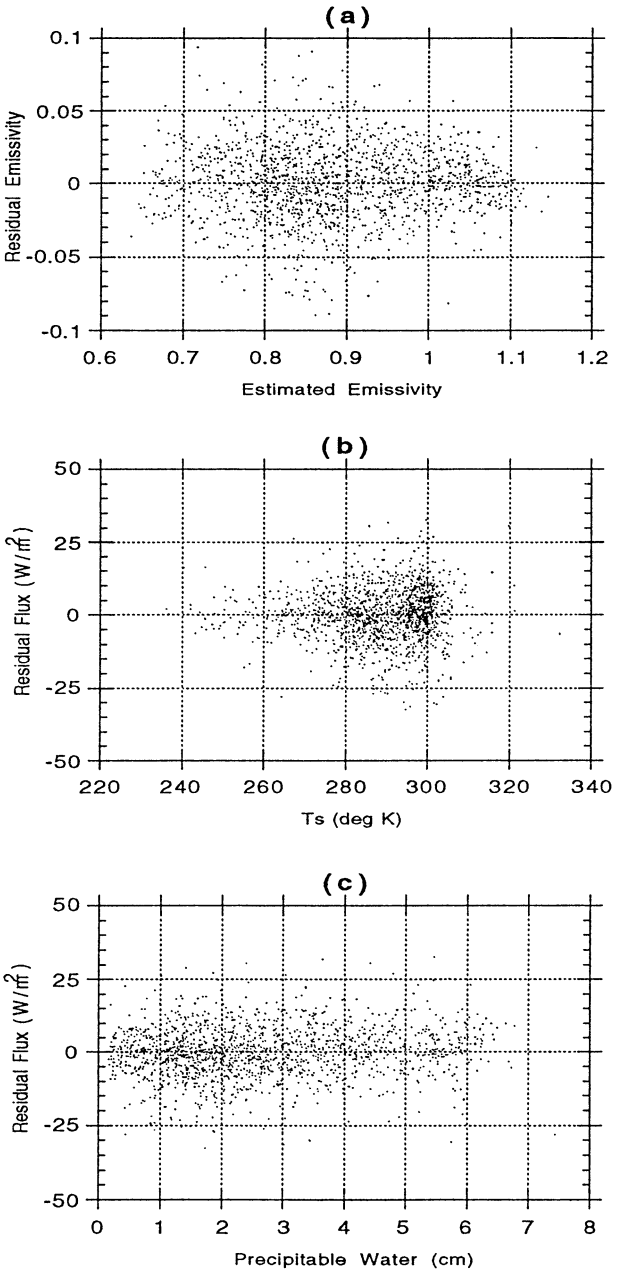

FIG. 4. Residual plots of the nonlinear model for clear skies (a) residual emissivity vs estimated emissivity [Eq. (15)]; (b) residual flux vs surface temperature; (c) residual flux vs precipitable water [Eq. (17)].

where b_{i,z_c} are regression coefficients. The overcast sky regressions were performed at 10 selected cloud-base heights. The overcast sky DLR estimate is obtained by combining the results from the Eqs. (17) and (23).

The rms DLR errors for the nonlinear model [Eqs. (17) and (23)] range from about 3 to 9 W m^{-2} (see Fig. 1). They are about 2 W m^{-2} lower than those from the linear model, and the distribution of the residuals has improved significantly. Figure 4 shows the residual plots for clear-sky conditions for the nonlinear model. One can see that the emissivity residuals are much more evenly distributed compared to that of the linear model (see Fig. 2), and the DLR residuals do not present obvious biases over the ranges of the surface temperature and water vapor. The linear model problem related to the hot-dry conditions disappeared as well. The residual plots for overcast conditions show similar results yet with smaller spreads. It is worth mentioning that the standard error of the estimated clear-sky DLR is about 9 W m^{-2}. This is the first model to estimate the clear-sky DLR using information from only HIRS observations that has a standard error within 10 W m^{-2}, which is considered the threshold accuracy for climate studies.

In summary, for clear and overcast conditions, the nonlinear model has DLR estimation errors of about 9 W m^{-2} for clear-sky conditions, and about 3 to 8 W m^{-2} for overcast conditions, depending upon cloud levels. These are about 1 to 3 W m^{-2} less than those of the linear model. Furthermore, while the linear model tends to underestimate the DLR in very moist conditions, the nonlinear model has evenly distributed residuals relative to the precipitable water. This suggests that this model will yield unbiased estimates from dry to moist conditions.

c. Surface pressure effects

The pressure dependence is primarily due to the effect of the pressure broadening of the spectral lines. The DLR calculations shown here are for surface pressure of 1000 hPa. Thus we have to make corrections due to changes in pressure broadening as the surface pressure departs significantly from 1000 hPa.

In order to simulate soundings above elevated surfaces, the Phillips et al. soundings were truncated at 900, 800, 700, 600, and 500 hPa. The intensity and flux calculations were repeated for each set of soundings, and the necessary regression coefficients were determined for each set of truncated surface pressure. Since it is very possible that only a few of the Phillips et al. soundings are from elevated stations, the method to adjust the soundings to represent the elevated area may cause errors.

Application of this inference technique to a given location requires knowledge of the surface pressure. When the surface pressure is not available, an estimate of the surface pressure is needed. The approach followed here was to use the hypsometric formula to estimate the surface pressure for a given elevation using one of the five Air Force Geophysics Laboratory (AFGL) standard soundings (McClatchey et al. 1972) according to the season and latitude.

4. Sensitivity study and error analysis

The estimate of total DLR is a function of HIRS radiances, effective cloud amount, cloud-base pressure

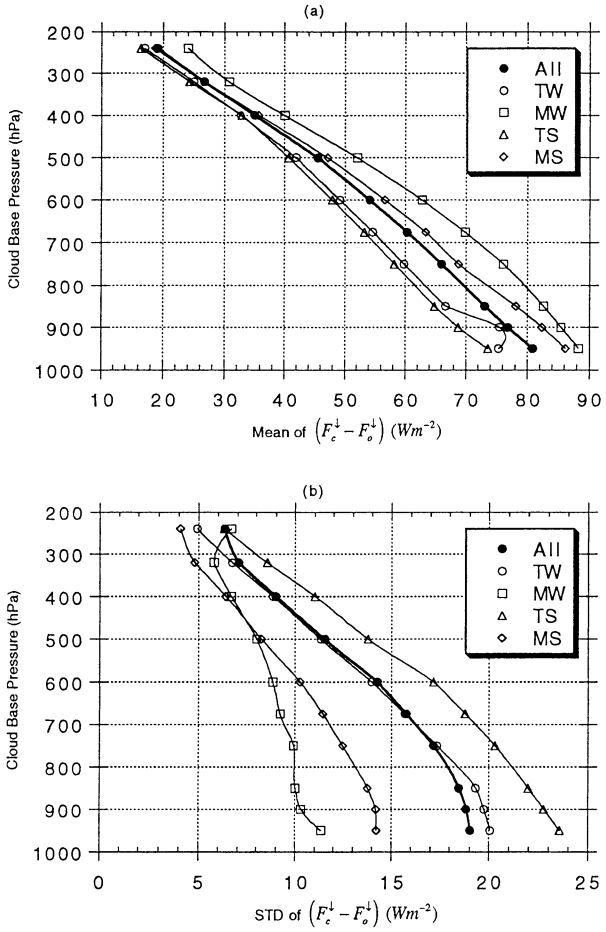

FIG. 5. Sensitivities of the DLR to a 100% error in the cloud amount. The legend symbols refer to all soundings (ALL), tropical winter (TW), midlatitude winter (MW), tropical summer (TS), and midlatitude summer (MS), respectively. Here, (a) and (b) are the mean values and standard deviations, respectively.

and the surface pressure. Based on Eq. (7), they are evaluated by the following expressions with the 1600 Phillips et al. soundings.

a. Sensitivity to cloud amount

The change of DLR with respect to a unit change in the cloud amount is

$$\frac{\partial \mathrm{DLR}}{\partial A} = F_c^{\downarrow} - F_o^{\downarrow} \tag{25}$$

The sensitivity of DLR to the uncertainties in cloud amount is expressed as

$$\delta \mathrm{DLR} = \delta A[\overline{(F_c^{\downarrow} - F_o^{\downarrow})} \pm \sigma(F_c^{\downarrow} - F_o^{\downarrow})], \tag{26}$$

where δA is the uncertainty of cloud amount, $\overline{(F_c^{\downarrow} - F_o^{\downarrow})}$ is the mean value of the DLR cloud radiative forcing and $\sigma(F_c^{\downarrow} - F_o^{\downarrow})$ is its standard deviation.

Figure 5a shows $\overline{(F_c^{\downarrow} - F_o^{\downarrow})}$ whose values represent the sensitivity of the total DLR to a 100% cloud amount uncertainty [see Eq. (25)]. It shows that the magnitude of the sensitivity decreases on average from about 80 to 20 W m^{-2} for the cloud-base pressures from 950 to 240 hPa. Figure 5a also shows the sensitivity of DLR to the cloud amount is largest during the midlatitude winter and the least for the tropical summer conditions, which occurs because there is less alternation of emission from a cloud by water vapor.

Figure 5b shows the standard deviation of the DLR cloud radiative forcing, ranging from about 5 to 25 W m^{-2}, or about 10%–30% of their respective mean values. It should be noted that in contrast to the mean values of the sensitivity study, the tropical summer cases have the largest variability while the midlatitude winter cases have the smallest.

b. Sensitivity to cloud-base pressure

The change of DLR with respect to a unit change in the cloud-base pressure, P_{cb}, at a unit cloud amount is

$$\frac{1}{A}\frac{\partial \mathrm{DLR}}{\partial P_{\mathrm{cb}}} = \frac{\partial F_c^{\downarrow}}{\partial P_{\mathrm{cb}}} \tag{27}$$

The DLR sensitivity to the uncertainties in cloud-base pressure can be written as

$$\delta \mathrm{DLR} = A\delta P_{\mathrm{cb}}\left\{\overline{\left(\frac{\partial F_c^{\downarrow}}{\partial P_{\mathrm{cb}}}\right)} \pm \sigma\left(\frac{\partial F_c^{\downarrow}}{\partial P_{\mathrm{cb}}}\right)\right\}, \tag{28}$$

where δP_{cb} is the uncertainty of cloud-base pressure in hPa, and $\overline{(\partial F_c^{\downarrow}/\partial P_{\mathrm{cb}})}$ and $\sigma(\partial F_c^{\downarrow}/\partial P_{\mathrm{cb}})$ are the mean and the standard deviation of $\partial F_c^{\downarrow}/\partial P_{\mathrm{cb}}$, respectively.

Figure 6a shows $(\overline{\partial F_c^{\downarrow}/\partial P_{\mathrm{cb}}} \times 100)$ assuming a 100-hPa uncertainty in the cloud-base pressure. The sensitivities range from about 6 to 12 W m^{-2} for the clouds with various base pressures. Figure 6b shows the standard deviation of $\partial F_c^{\downarrow}/\partial P_{\mathrm{cb}}$ for the same conditions, a measure of the range of the DLR sensitivity variation to the uncertainties in the cloud-base pressure. Notice that the standard deviation values for clouds lower than 800 hPa are about the same magnitude as their means. This suggests that, for low clouds, the DLR has broader ranges of sensitivity to cloud-base uncertainties. In other words, for low clouds, even if the magnitude of errors in estimating cloud-base pressure were relatively constant, the DLR may still have a wide range of errors.

c. Sensitivity to surface pressure

The change of DLR with respect to a unit change in the surface pressure, P_{S}, is

$$\frac{\partial \mathrm{DLR}}{\partial P_s} = (1 - A)\frac{\partial F_o^{\downarrow}}{\partial P_s} + A\frac{\partial F_c^{\downarrow}}{\partial P_s}, \tag{29}$$

where $\partial F_o^{\downarrow}/\partial P_s$ and $\partial F_c^{\downarrow}/\partial P_s$ are the changes of the DLR corresponding to the change of the surface pressure in clear-sky and overcast conditions, respectively.

Figures 7a,b show the mean and standard deviation

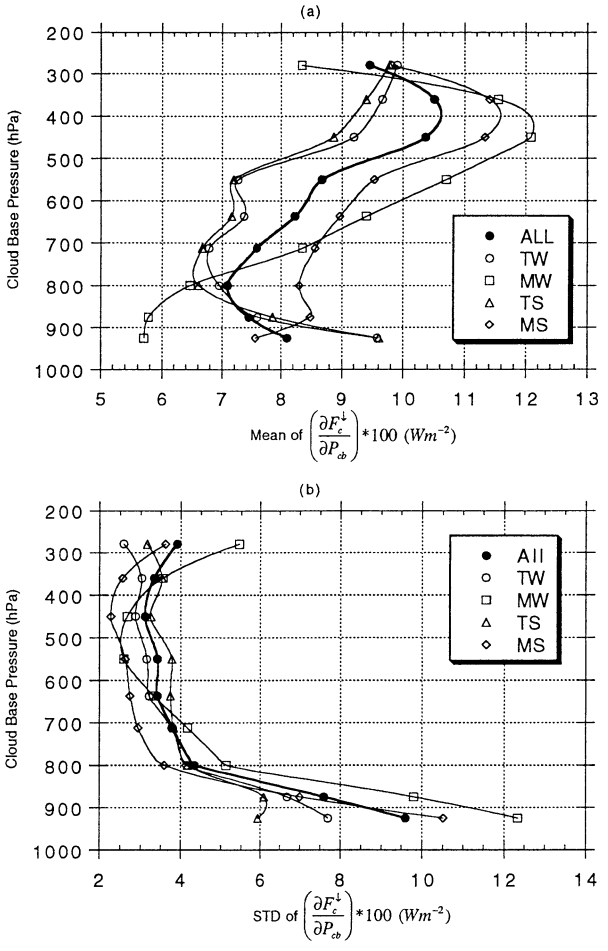

FIG. 6. Sensitivities of the DLR due to the errors in the cloud-base pressures for different average atmospheric conditions. Here, (a) and (b) are the mean values and standard deviations with a 100-hPa uncertainty in the cloud-base pressures, respectively.

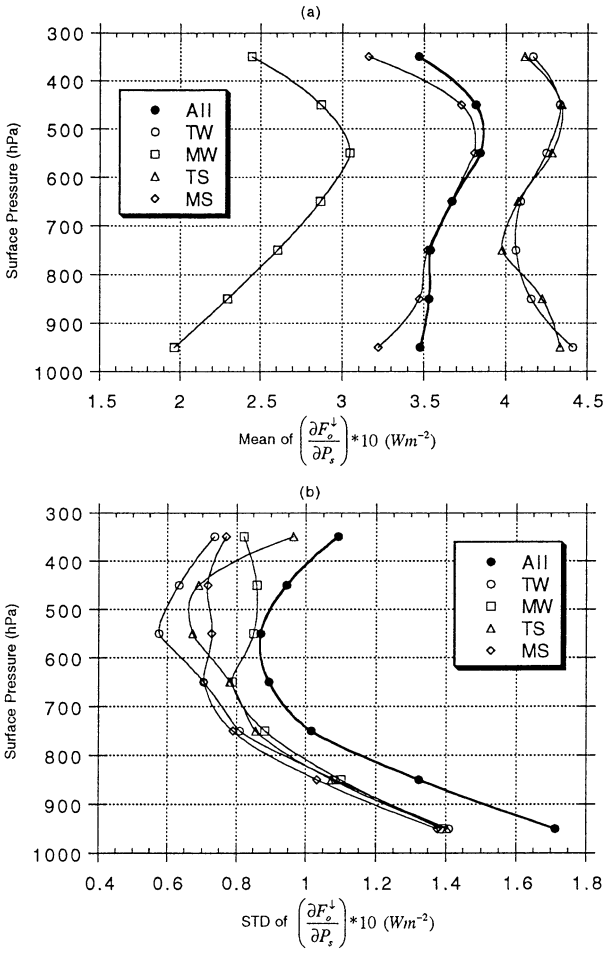

FIG. 7. Sensitivities of the clear-sky DLR due to the errors in the surface pressures. Here, (a) and (b) are the mean values and standard deviations, respectively, with a 10-hPa uncertainty in the surface pressures.

of $\partial F_o^{\downarrow}/\partial P_s$ scaled by 10—the sensitivity of the clear-sky DLR to a 10-hPa uncertainty in the surface pressure. The mean sensitivity is about 4 W m^{-2} with a variability of 1 to 2 W m^{-2}. For partly cloudy conditions, the sensitivity is about 3 W m^{-2} on average for every 10-hPa uncertainty in the surface pressure.

d. Sensitivity to radiance noise

We generated several independent sets of normally distributed random noise for each relevant HIRS channel based on the Nominal Equivalent Differential Radiance (NEΔN) listed in the *NOAA Polar Orbiter Data Users' Guide* (NOAA 1995). The regression analysis was performed repeatedly with the corresponding noise added to the radiance of HIRS channels. The change of rms regression errors is considered a measure of the sensitivity to instrument noise. For the linear model under the clear skies, the rms regression errors increased by about 6 W m^{-2} from about 12 W m^{-2} for noise-free conditions. For the nonlinear clear-sky model, the rms regression errors merely increased by about 0.5 W m^{-2} from 8.7 W m^{-2}. This is further evidence that the nonlinear model is better than its linear counterpart. The nonlinear model has a smaller rms regression error, and is much less sensitive to noise than the linear one.

For overcast conditions, the increases of the rms regression errors of the nonlinear model are all within 1 W m^{-2} when the instrument noise is included.

e. Sensitivity to clear-column radiance errors

Since this DLR estimation technique requires the clear-column radiances, it is subject to the uncertainties in the retrieval processes if clear-column radiances are not observed directly. It should be pointed out that these uncertainties affect all methods that calculate DLR using satellite meteorological data as input. Because an estimate of the accuracy of the retrieval processes for obtaining clear-column radiances cannot be found in the

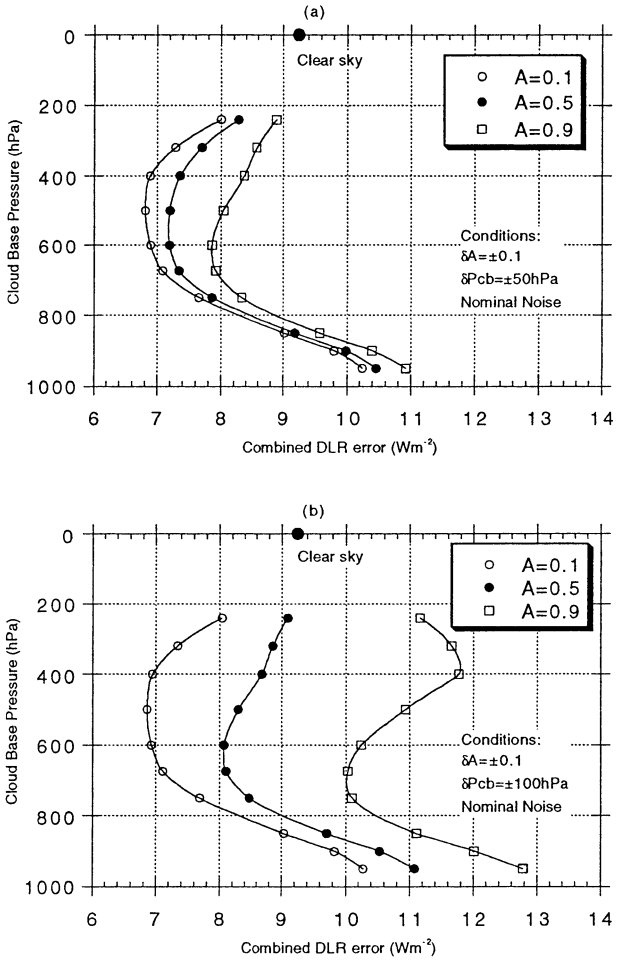

FIG. 8. Combined DLR errors contributed from regression error and the errors from the uncertainties in cloud amounts and cloud-base heights. Curves are shown for the indicated cloud amounts. Different degrees of uncertainties in cloud parameters are considered: (a) $\delta A = \pm 10\%$ and $\delta P_{cb} = \pm 50$ hPa, and (b) $\delta A = \pm 10\%$ and $\delta P_{cb} = \pm 100$ hPa.

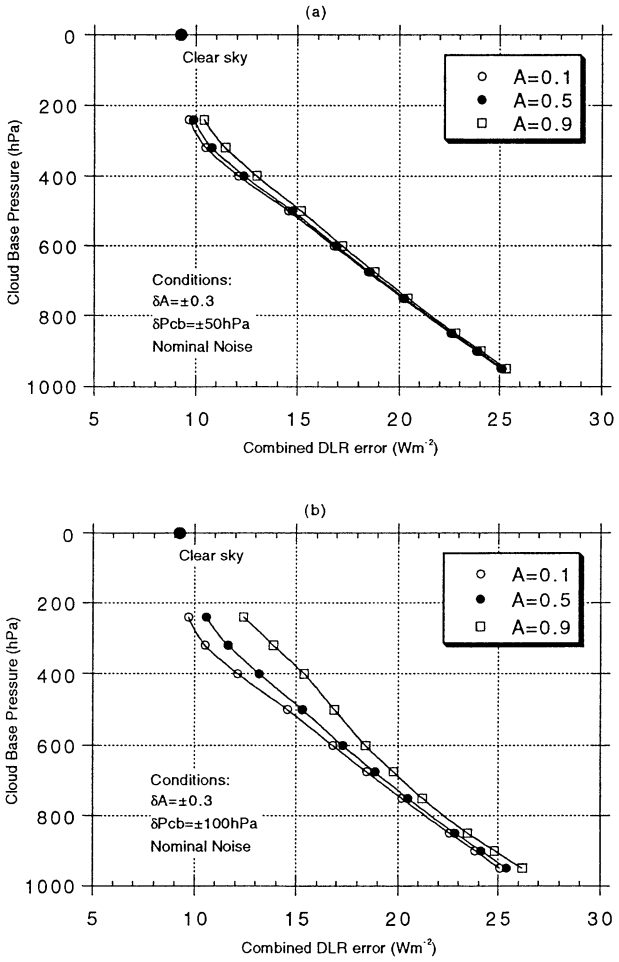

FIG. 9. As in Fig. 8 but for (a) $\delta A = \pm 30\%$ and $\delta P_{cb} = \pm 50$ hPa, and (b) $\delta A = \pm 30\%$ and $\delta P_{cb} = \pm 100$ hPa.

literature, we leave the estimation of this effect for future research.

f. Combined effects

To estimate the combined effects of all errors mentioned earlier, we assume the error components are independent. We estimate the combined effects by the square root of the sum of the squares of the errors of all the components.

Figures 8 and 9 show the combined DLR errors due to errors from regression (noise included) and uncertainties in cloud amount and cloud-base pressure at various cloud amounts. The results in Figs. 8a,b were calculated for a 10% cloud amount uncertainty with ± 50 hPa and ± 100 hPa cloud-base pressure uncertainties, respectively. Figures 9a,b were calculated for a 30% cloud amount uncertainty with ± 50 hPa and ± 100 hPa cloud-base pressure uncertainties, respectively. There are some common features in these four plots. First, the combined DLR error increases with the cloud amount, as expected from Eq. (28). Also notice that the DLR errors are generally larger when the cloud bases are at higher pressures. When the cloud amount uncertainty reaches 30%, its effect dominates the DLR errors and therefore the contributions from other error sources, for example, uncertainty in the cloud-base pressure make relatively small differences in the total DLR errors.

g. Other effects

Other potential error sources pertaining to this DLR estimation technique include the soundings used for the regression analyses and the radiative transfer model used for the calculations. We assume that the Phillips et al. soundings are representative of the distribution of meteorological conditions for areas ranging from the Tropics to midlatitudes. However, there are no very cold and dry soundings since the dataset does not contain soundings from latitudes higher than 60°. The DLR es-

timation in polar regions must be considered as an extrapolation. In addition, while climatological ozone profiles were used, the estimated DLR for a set of observed radiances will have some error since the actual ozone profile is not included. However, since the ozone contribution to the mean total DLR is only a few W m^{-2}, the error due to inconsistent ozone concentration is small compared to other error sources.

The radiation model used in this study has been validated with line-by-line model calculations and observations that demonstrated a flux difference to within 2% (Ellingson and Serafino 1984). Fluxes calculated with the recently improved model agree with the line-by-line radiative transfer model (LBLRTM) to about 1 W m^{-2} for the entire vertical range of the atmosphere for several cases (Warner and Ellingson 2000). Also, the outgoing longwave radiation estimation scheme based on this radiation model using a similar technique was shown to be successful (Ellingson et al. 1994). We believe that the relative error from the radiative transfer model calculations is small. However, if the DLR estimate is biased, it may be attributed to the radiation calculations. Extensive, additional validation of the model will be performed with ARM measurements.

Although the technique may be biased due to the choice of radiation model, the same can be said for any inference technique. The results shown here demonstrate the validity of the approach. Modifications to account for improvement in spectral absorption parameters are relatively easy to compute.

One should note the difference between systematic error and random errors. The assessment of error sources discussed herein is valid for either systematic or random errors. However, when the number of observations increases, the random error diminishes by the inverse of the square root of the number of observations, while the systematic error is constant. One good example of an error source is the cloud amount where both systematic and random errors are commonly present and sometimes, in equivalent magnitudes.

Overall, the DLR estimation error, excluding the contribution due to the error in the surface pressure, ranges from about 7 to 12 W m^{-2} when there is a $\pm 10\%$ uncertainty in cloud amounts and a ± 100 hPa uncertainty in cloud-base pressure. When the cloud amount uncertainty rises to 30%, the range of the combined DLR error increases to about 10 to 25 W m^{-2}. Note that the error of TOVS-derived cloud amount is estimated to be 20% (NOAA 1995).

5. Preliminary validation results

The DLR estimation algorithm was examined for clear-sky conditions based on radiative transfer model simulations over a wide range of atmospheric and geographical conditions. The DLR and HIRS radiances were calculated with the RGE radiative transfer model using analyses from the Global Data Assimilation System (GDAS) at the National Centers for Environmental Prediction (NCEP). We refer to this DLR as the calculated DLR. The globally distributed satellite estimate of DLR (referred to as estimated DLR) was calculated with the nonlinear regression model using the simulated HIRS radiances. The NCEP analysis fields were provided on a 2.18° lat by 2.22° lon grid (162×82 grid points globally) at 19 vertical sigma levels and four synoptic hours a day. The earth's skin temperatures and surface pressures were also provided. We used the data from 0000 UTC 22 December 1990 for this validation study.

As mentioned in section 3c, a surface pressure field was generated based on an elevation map from NCEP analyses with the relationship determined by the hypsometric formula using the AFGL standard soundings for tropical, midlatitude, and polar areas. This is referred to as the estimated surface pressure, which provides a test bed when the surface pressure is not available.

Figure 10 shows the global distribution of the clear-sky DLR calculated by the RGE radiative transfer model using the 0000 UTC 22 December 1990 NCEP analyses. This is assumed to be the ''ground truth'' for this validation purpose. Patterns can be readily recognized to relate to the surface temperature distribution, such as near-zonal distribution of DLR over the oceans, orographic dependence, and the colder continents in the Northern Hemisphere.

The estimated DLR field using either the NCEP or the estimated surface pressure greatly resembles the calculated one. Hereon, we will limit our discussion to the estimated DLR using the NCEP surface pressures unless otherwise noted, although the discussion is generally true for either estimate. The corresponding global distribution of the DLR differences (estimated minus calculated) is shown in Fig. 11. This figure shows that contours exceeding ± 10 W m^{-2} are relatively sparsely distributed and no obvious correlation with geographical or meteorological features can be observed. However, large areas of underestimation can be found in latitudes poleward of about 60°S, especially over the oceans surrounding Antarctica. Some areas with large overestimation are also found to the west of continents near 30°S. The causes for these two problems are not known.

Some differences can be related to the sharp temperature discontinuity near the surface, for example, in the northern Atlantic near Greenland, western Australia, the Tibetan Plateau, and parts of the Sahara and Saudi Arabia. Since the NCEP skin temperatures were used as the ground-level temperatures in the radiation calculation, large DLR estimation errors occur when the skin temperature is very different from the surface air temperature. For these cases, the DLR estimation errors may be caused by the errors in the NCEP skin temperatures and/or that the DLR estimation algorithm fails to give correct results under such circumstances. The distribution of the DLR estimation errors is very close to a normal distribution when the southernmost 30° lati-

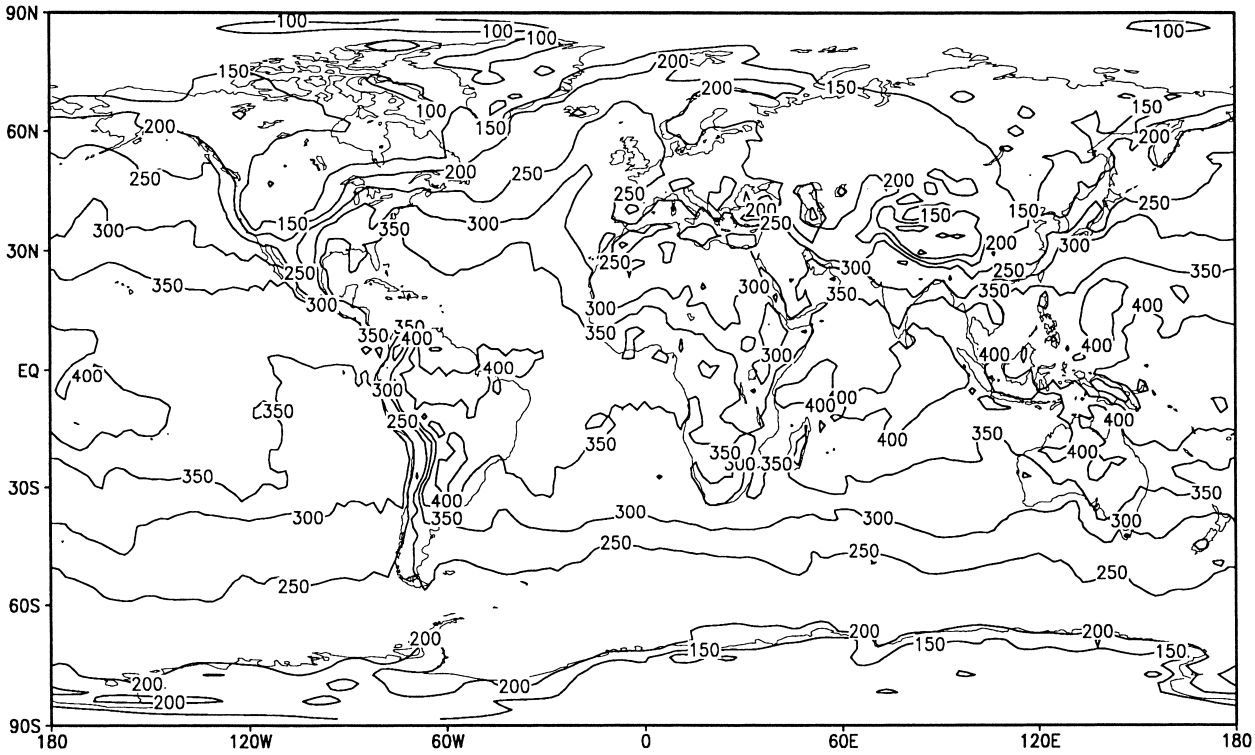

FIG. 10. Global distribution of the clear-sky DLR calculated by the RGE radiative transfer model using the 0000 UTC 22 Dec 1990 NCEP analysis. The contour interval is 50 W m^{-2}.

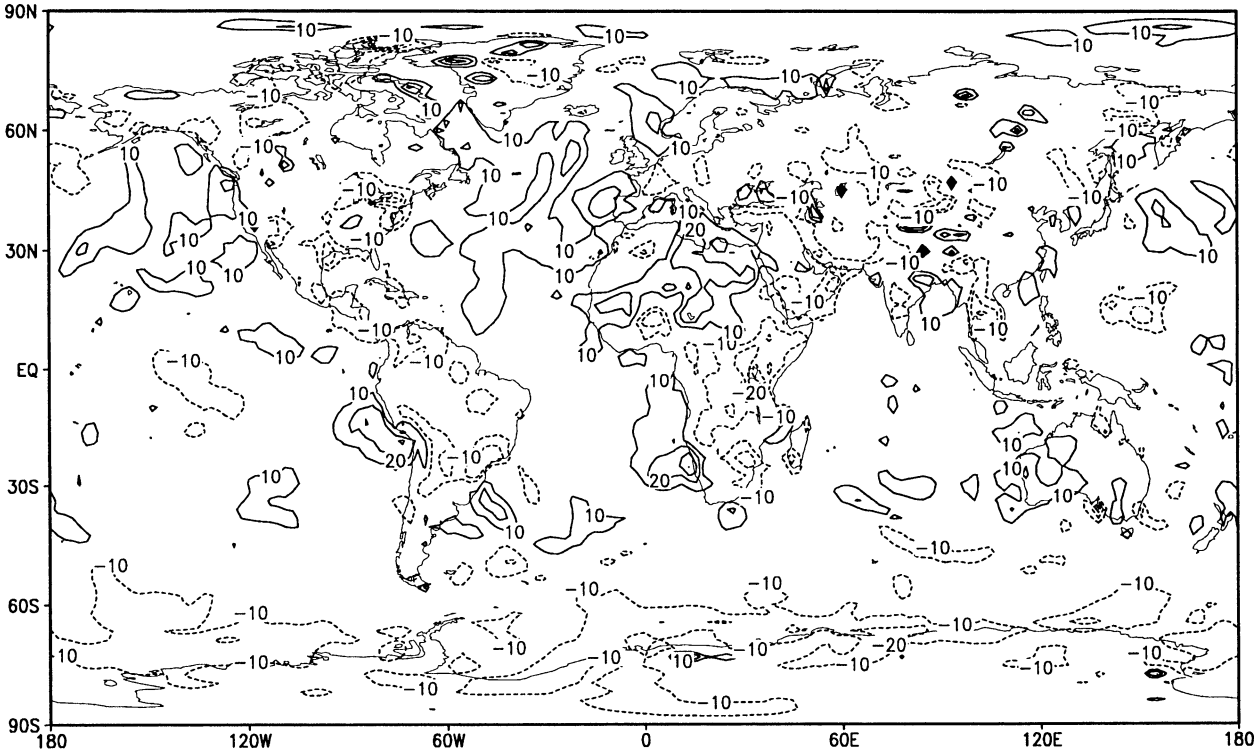

FIG. 11. Global distribution of the estimated minus calculated DLR (W m^{-2}) for 0000 UTC 22 Dec 1990. The contour interval is 10 W m^{-2} with the 0 W m^{-2} contour omitted for improved visualization purposes.

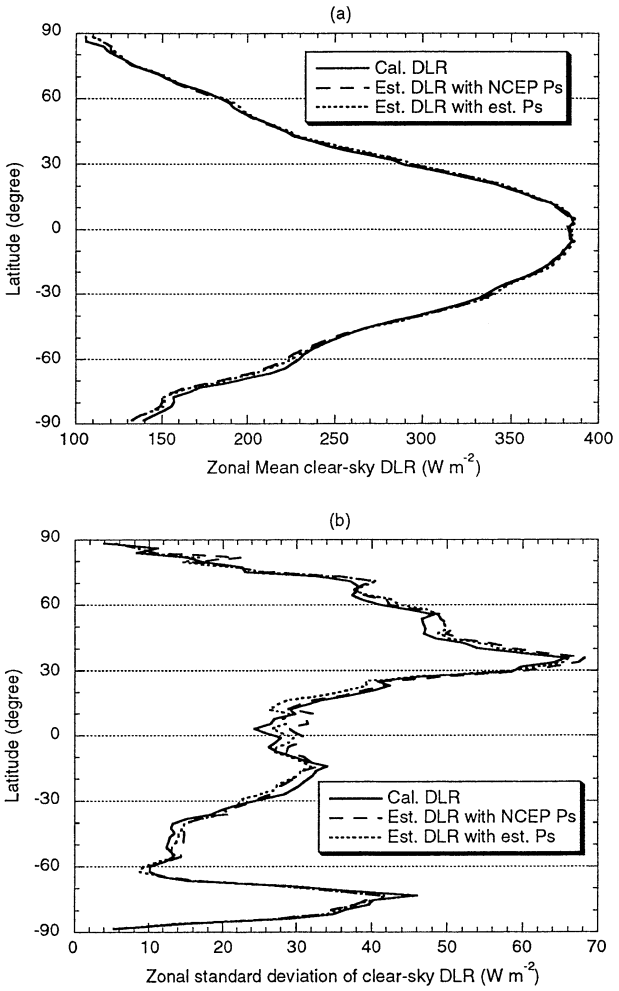

FIG. 12. Zonal statistics of the calculated (solid) and estimated [(dashed) with NCEP surface pressure; and (dotted) with estimated surface pressure] DLR (W m^{-2}) for 0000 UTC 22 Dec 1990. Here, (a) zonal mean, and (b) zonal standard deviation.

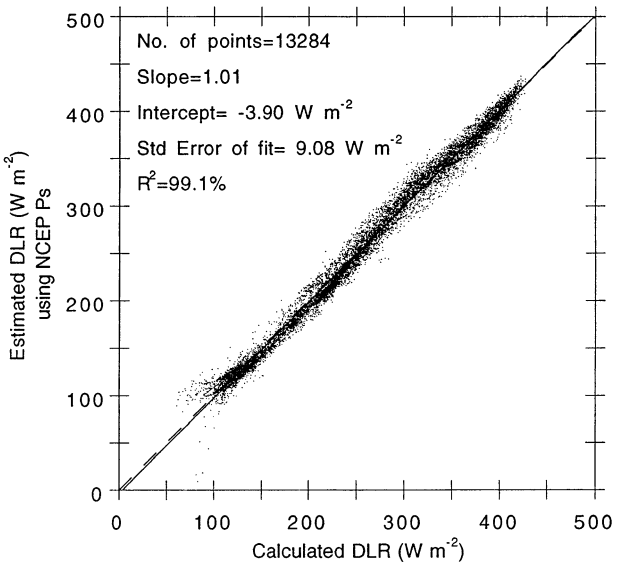

FIG. 13. Estimated DLR using NCEP surface pressure vs the calculated DLR for 0000 UTC 22 Dec 1990. The diagonal solid line is the slope of the fit and it overlays closely the perfect fit line (dashed).

tudinal zone is excluded. For the 162 × 82 grid boxes, about 75% of them are within ±10 W m^{-2} and about 91% of them are within ±15 W m^{-2}. It should be noted that these errors are for instantaneous estimates. Random errors are expected to be lower for monthly averages.

Figures 12a,b show the zonal means and standard deviations for the calculated and estimated DLR. The differences of zonal means between the calculated and either estimate are within ±5 W m^{-2} with the exception of high latitudes, particularly in the Southern Hemisphere. The reproduction of the variability of an estimate is also important. Figure 12b shows the HIRS estimates have reproduced the variability to within ±5 W m^{-2}. These zonal statistics are very good in general, and this is very encouraging for the applicability of this technique.

Figure 13 shows a scatterplot of the estimated versus the calculated DLR. The correlation coefficient is 0.996, and the explained variance is 99.1%. The most encouraging feature, besides the quite uniform scatter throughout the range, is that the estimates at both ends are unbiased. The ranges of temperatures and the water vapor variations in the Phillips et al. soundings are smaller than those of the NCEP analyses, particularly the moisture. The extension of this estimation technique into those meteorological conditions without significant bias is considered a great success. This indicates that the physics has been appropriately embedded in the regression model formulation.

The points that show large underestimation on the lower left corner in Fig. 13 were found to be from Ellesmere Island, Canada (an island to the west of Greenland). The NCEP surface pressure field shows a very low pressure center (<850 mb) whose location coincides with this large DLR underestimation. Examination of the DLR error against the elevation showed that the DLR was underestimated consistently by about 10 W m^{-2} for the most elevated regions. This suggests that we need to improve the methodology to better include the surface pressure effects.

Overall, the mean DLR differences are 0.0 and 1.8 W m^{-2} when the estimations are made with NCEP and estimated surface pressure fields, respectively. Since the simulations are self-consistent, zero bias in the estimate is expected. The 1.8 W m^{-2} bias of the DLR estimate using the estimated surface pressure must be due to the errors in surface pressure estimation. The standard deviations of the DLR differences are 9.2 and 9.1 W m^{-2} for the two estimates, respectively. Using the F-test, we found that the variance of the validation errors is not significantly greater than that of the regression. This gives us confidence to apply this algorithm to real data.

Ultimately, we need to compare satellite-estimated DLR to surface observations since only then can the algorithm be better characterized. This is left for future study.

6. Concluding remarks

The surface energy budget plays an important role in determining many atmospheric and oceanic processes, especially on the large scale. The DLR at the earth's surface is one of the components necessary to study the surface energy budget. It is very difficult to study the global distribution of the DLR using ground observations because observations are sparse or nonexistent, particularly over the oceans. This paper developed a technique to directly use satellite radiance observations to estimate the DLR.

Both linear and nonlinear regression models were developed. The rms regression errors of the linear model range from about 5 to 13 W m^{-2}, whereas the rms regression errors of the nonlinear model range from about 3 to 9 W m^{-2}. The nonlinear model errors are about 1 to 3 W m^{-2} lower than those of the linear model for clear sky and overcast conditions. For clear-sky conditions, when the effects of noise are included, the rms error of the linear model increases by about 6 W m^{-2} while that of nonlinear model increases by only 0.5 W m^{-2}. For clear sky and overcast conditions, when instrument noise is included, the rms regression errors of the nonlinear model range from about 4 to 9 W m^{-2}. Most importantly, the nonlinear model showed an unbiased estimate over the entire range of meteorological conditions.

Sensitivity studies were performed for major error sources, including the cloud amount, cloud-base pressure, and surface pressure. On average, the DLR is most sensitive to the error in the cloud amount. Overall, the combined DLR error, excluding the effects of the surface pressure errors, ranges from about 7 to 12 W m^{-2} when there is a $\pm 10\%$ uncertainty in cloud amounts and a ± 100 hPa uncertainty in cloud-base pressures. When the cloud amount uncertainty rises to 30%, the combined DLR error ranges from about 10 to 25 W m^{-2}.

The nonlinear clear-sky DLR estimation technique was preliminarily validated using simulated radiation data. The DLR estimates were determined using both NCEP and empirically estimated surface pressures. Both estimates were compared with the DLR calculated from the radiation model. The standard deviation of the estimated minus calculated DLR is about 9 W m^{-2} using either surface pressure field, with the mean differences of about 0 and 2 W m^{-2}, using NCEP and estimated surface pressures, respectively. While this estimation technique works relatively well over the ocean, we have found that the DLR was systematically underestimated by about 10 W m^{-2} for more elevated regions. This problem may be caused by improper simulations of the DLR for elevated regions and by an incorrect method to account for surface pressure effects. This suggests that we may need to collect balloon soundings from elevated stations and consider another method to better account for the surface pressure effects. We also noticed problems associated with the surface temperature discontinuities. This suggests the need to find an additional mechanism to handle near-surface inversions and strong vertical temperature gradients near the surface.

Since the NOAA polar orbiting satellites only pass over most areas twice per day (except high latitudes where the satellite swaths overlap), there are possible sampling errors for the DLR estimation due to the nonsinusoidal OLR diurnal variation. This temporal sampling error for OLR has been demonstrated by Ba and Ellingson (2000) using OLR derived from geostationary satellite observations. Similar studies can be performed for the DLR. Surface observations could also be used for this purpose, however, the spatial distribution is relatively limited.

The cloud-base pressure and the effective cloud amount are needed for application to cloudy conditions. We expect the cloud information to be provided from other satellite cloud algorithms. Such satellite-derived cloud-base information is not operationally produced. We are looking into algorithms developed under Clouds from Advanced Very High Resolution Radiometer (CLAVR) and Moderate Resolution Imaging Spectroradiometer (MODIS) as possible cloud information sources. The cloudy-sky DLR algorithm may need to be modified and adapted to the cloud information that is actually used. The effects on the DLR using different cloud data sources, however, have not been examined. This is the most important study remaining before this technique can be implemented. Since the sensitivity study shows that the DLR error due to uncertainties of the cloud amount usually dominates the other error components, accurate cloud amount estimates are most important for cloudy-sky DLR estimation. Nonetheless, the effects of the uncertainties of the cloud-base pressure are not negligible.

Despite the limitations noted above, our analysis indicates that the statistical method developed in this study should provide instantaneous estimates of the DLR to within about 10 W m^{-2} rms directly from the HIRS observations if the cloud amount and base pressure can be accurately estimated, that is, about a $\pm 10\%$ uncertainty in cloud amounts and about a ± 100 hPa uncertainty in cloud-base pressures. In addition, it is expected that the errors will be considerably smaller for monthly averages, except where persistent extreme conditions occur. Furthermore, the technique is computationally inexpensive—the DLR may be estimated with less than fifty arithmetic operations as compared to thousands by even a broadband radiation model. The necessary coefficients for this algorithm are available from the authors upon request.

Acknowledgments. This research was supported in part by National Oceanic and Atmospheric Administration through the Cooperative Institute for Climate Studies, and by the National Aeronautics and Space Administration under Grants NAGW-1471, S4 and NAG5-6483. The authors would like to express their gratitude to the three anonymous journal reviewers for providing valuable comments and suggestions.

REFERENCES

Augustine, J. A., J. J. DeLuisi, and C. N. Long, 2000: SURFRAD—A national surface radiation budget network for atmospheric research. *Bull. Amer. Meteor. Soc.,* **81,** 2341–2358.

Ba, M., and R. G. Ellingson, 2000: A study of diurnal cycle of OLR using GOES sounder data. *IRS 2000: Current Problems in Atmospheric Radiation,* W. L. Smith and Y. M. Timofeyev, Eds., A. Deepak, 505–508.

Clough, S. A., F. X. Kneizys, and R. W. Davies, 1989: Line shape and the water vapor continuum. *Atmos. Res.,* **23,** 229–241.

Darnell, W. L., S. K. Gupta, and W. F. Staylor, 1983: Downward longwave radiation at the surface from satellite measurements. *J. Appl. Meteor.,* **22,** 1956–1960.

——, ——, and ——, 1986: Downward longwave surface radiation from sun-synchronous satellite data: Validation of methodology. *J. Climate Appl. Meteor.,* **25,** 1012–1021.

Dedieu, G., P. Y. Deschamps, and Y. H. Kerr, 1987: Satellite estimation of solar irradiance at the surface of the earth and the surface albedo using a physical model applied to METEOSAT data. *J. Climate Appl. Meteor.,* **26,** 79–87.

Ellingson, R. G., 1982: On the effects of cumulus dimensions on longwave irradiance and heating rate calculations. *J. Atmos. Sci.,* **39,** 886–896.

——, 1995: Surface longwave fluxes from satellite observations: A critical review. *Remote Sens. Environ.,* **51,** 89–97.

——, and J. C. Gille, 1978: An infrared radiative transfer model. Part I: Model description and comparison of observations with calculations. *J. Atmos. Sci.,* **35,** 523–545.

——, and R. R. Ferraro, 1983: An examination of a technique for estimating the longwave radiation budget from satellite radiance observations. *J. Climate Appl. Meteor.,* **22,** 1416–1423.

——, and G. N. Serafino, 1984: Observations and calculations of aerosol heating over the Arabian Sea during MONEX. *J. Atmos. Sci.,* **41,** 575–589.

——, D. J. Yanuk, H.-T. Lee, and A. Gruber, 1989: A technique for estimating outgoing longwave radiation from HIRS radiance observations. *J. Atmos. Oceanic. Technol.,* **6,** 706–711.

——, J. Ellis, and S. Fels, 1991: The intercomparison of radiation codes in climate models (ICRCCM): Longwave results. *J. Geophys. Res.,* **96,** 8929–8953.

——, H.-T. Lee, D. Yanuk, and A. Gruber, 1994: Validation of a technique for estimating outgoing longwave radiation from HIRS radiance observations. *J. Atmos. Oceanic. Technol.,* **11,** 357–365.

Frouin, R., and C. Gautier, 1988: Downward longwave irradiance at the ocean surface from satellite data: Methodology and in situ validation. *J. Geophys. Res.,* **93,** 597–619.

Fung, I., D. E. Harrison, and A. Lacis, 1984: On the variability of the net longwave radiation at the ocean surface. *Rev. Geophys.,* **22,** 177–193.

Gautier, C., G. Diak, and S. Masso, 1980: Simple physical model to estimate incident solar radiation from GOES satellite data. *J. Appl. Meteor.,* **19,** 1005–1012.

Gupta, S. K., 1989: A parameterization of longwave radiation from sun-synchronous satellite data. *J. Climate,* **2,** 305–320.

——, W. L. Darnell, and A. C. Wilber, 1992: A parameterization for longwave surface radiation from satellite data: Recent improvements. *J. Appl. Meteor.,* **31,** 1361–1367.

——, A. C. Wilber, W. L. Darnell, and J. T. Suttles, 1993: Longwave surface radiation over the glove from satellite data: An error analysis. *Int. J. Remote Sens.,* **14,** 95–114.

——, N. A. Ritchey, A. C. Wilber, C. H. Whitlock, G. G. Gibson, and P. W. Stackhouse Jr., 1999: A climatology of surface radiation budget derived from satellite data. *J. Climate,* **12,** 2691–2710.

Hicks, B. B., J. J. DeLuisi, and D. Matt, 1996: The NOAA Integrated Surface Irradiance Study (ISIS): A new surface radiation monitoring network. *Bull. Amer. Meteor. Soc.,* **77,** 2857–2864.

IMSL, 1989: User's Manual. IMSL Library, FORTRAN Subroutines for Statistical Analysis, IMSL, Houston, TX, 1579 pp.

Lee, H.-T., 1993: Development of a statistical technique for estimating the downward longwave radiation at the surface from satellite observations. Ph.D. dissertation, University of Maryland, College Park, 150 pp.

Malkmus, R., 1967: Random Lorentz band model with exponential-tailed S-1 line intensity distribution function. *J. Opt. Soc. Amer.,* **57,** 323–329.

McClatchey, R. A., R. W. Fenn, J. E. A. Selby, F. E. Volz, and J. S. Garing, 1972: Optical Properties of the Atmosphere. 3d. ed. Air Force Cambridge Research Laboratories, Environmental Research Papers, ARCRL-72-0497, 108 pp.

McMillin, L. M., 1978: An improved technique for obtaining clear radiance from cloud contaminated radiances. *Mon. Wea. Rev.,* **106,** 1590–1597.

——, and C. Dean, 1982: Evaluation of a new technique for producing clear radiances. *J. Appl. Meteor.,* **21,** 1005–1014.

Meerkoetter, R., and H. Grassl, 1984: Longwave net flux at the ground from radiances at the top. *IRS'84: Current Problems in Atmospheric Radiation,* G. Fiocco, Ed., A. Deepak, 220–223.

Morcrette, J. J., and P. Y. Deschamps, 1986: Downward longwave radiation at the surface in clear sky atmospheres: Comparison of measured, satellite-derived and calculated fluxes. *Proc. ISLSCP Conf.,* Rome, Italy, ESA SP-248, 257–261.

NOAA, 1995: Polar orbiter data user's guide. Satellite Service Data Division, NCDC, NESDIS.

Ohmura, A., and Coauthors, 1998: Baseline Surface Radiation Network (BSRN/WRMC), a new precision radiometry for climate research. *Bull. Amer. Meteor. Soc.,* **79,** 2115–2136.

Phillips, N., J. Susskind, and L. McMillin, 1988: Results of a joint NOAA/NASA sounder simulation study. *J. Atmos. Oceanic Tech.,* **5,** 44–56.

Pinker, R. T., and L. A. Corio, 1984: Surface radiation budget from satellite. *Mon. Wea. Rev.,* **112,** 209–215.

Schmetz, J., 1989: Towards a surface radiation climatology: Retrieval of downward irradiances from satellites. *Atmos. Res.,* **23,** 287–321.

Schmetz, P., J. Schmetz, and E. Raschke, 1986: Estimation of daytime downward longwave radiation at the surface from satellite and grid point data. *Theor. Appl. Climatol.,* **37,** 136–149.

Smith, W. L., and H. M. Woolf, 1976: The use of eigenvectors of statistical covariance matrices for interpreting satellite sounding radiometer observations. *J. Atmos. Sci.,* **33,** 1127–1140.

——, and ——, 1983: Geostationary satellite sounder (VAS) observations of longwave radiation flux. Paper presented at the Satellite Systems to Measure Radiation Budget Parameters and Climate Change Signals, Iglis, Austria, International Radiation Commission.

Stokes, G. M., and S. E. Schwartz, 1994: The Atmospheric Radiation Measurement (ARM) program: Programmatic background and design of the cloud and radiation test bed. *Bull. Amer. Meteor. Soc.,* **75,** 1201–1221.

Tarpley, J. D., 1979: Estimating incident solar radiation at the surface from geostationary satellite data. *J. Appl. Meteor.,* **18,** 1172–1181.

Warner, J. X., and R. G. Ellingson, 2000: A new narrowband radiation model for water vapor absorption. *J. Atmos. Sci.,* **57,** 1481–1496.

WCRP-5, 1988: Concept of the Global Energy and Water Cycle Experiment. Report of the JSC study group, WMO/TD-N215, 63 pp.